Deep-inelastic spin and flavor asymmetry of the nucleon from a QCD-inspired quark model

Z. Dziembowski, C. J. Martoff, and P. Żyła
Department of Physics, Temple University, Philadelphia, Pennsylvania 19122
(Received 27 October 1993)

A systematic procedure is described which permits the structure functions of nucleons to be calculated from a nonrelativistic constituent quark model. Transformation from the nucleon rest frame to the light cone or infinite momentum frame is accomplished based on work of Susskind, which does not require the weak binding and nonrelativistic kinematical approximations used in previous work. The light-cone distribution functions so obtained are then subjected to QCD evolution, giving predictions for the quark momentum densities. The model incorporates SU(6) breaking by the QCD-inspired one gluon exchange potential originated by De Rújula, Georgi, and Glashow, with the parameters fixed by Isgur and Karl from the N-Δ mass splitting. In contrast with some previous work, the parameter values which fit the baryon mass spectrum are here shown to also give rather good agreement with the deep-inelastic flavor and spin asymmetries in the valence region.

PACS number(s): 13.60.Hb, 12.39.Jh, 14.20.Dh

I. INTRODUCTION

It was a set of experiments at SLAC in the late 1960s on deep-inelastic scattering from proton and deuterium targets that showed the nucleon to be made of pointlike objects. Further studies with neutrinos, polarized electrons, and muons established the spin, charge, and baryon number of the pointlike objects and showed they were quarks. It was also recognized that these experiments not only detect quarks but directly measure their distribution within the target. In more technical terms, they measure various *light-cone or infinite momentum frame* (IMF) *quark correlation functions* in the target ground state [1]. If the wave functions of valence quarks were taken from a naive static quark model with the SU(6) symmetry built in, the F_2^n/F_2^p ratio and the nucleon spin asymmetry would be independent of Bjorken x. Experiments show clearly that these quantities are in fact strongly x dependent. These observed inhomogeneities mean that quarks with different quantum numbers are distributed differently within the nucleon. The purpose of this paper is to explore a possible dynamical origin for the observed inhomogeneities in nucleon structure [2].

The mass splittings in the ground-state baryon multiplet of course show that there is significant spin and flavor dependence in the internal structure of baryons. It has been shown that the mass splittings can be well reproduced by a nonrelativistic constituent quark model (NCQM) incorporating a perturbing potential of the form expected from one gluon exchange (OGEP) in QCD [3, 4]. In this paper we employ the constituent quark wave function from this model to calculate the observables of deep inelastic electron- (or muon-)nucleon scattering.

Indeed, it is physically reasonable that nonrelativistic physics should dominate the measured structure function ratios at moderate x. Recall that the valence quark distributions are peaked at Bjorken $x \simeq 1/3$ and vanish at $x = 0$ and $x = 1$, while the sea quarks and gluons tend to populate the small-x region. The limit $x \to 0$ generally implies very large parton momentum in the proton rest frame while $x \simeq 1/3$ implies a particle with nonrelativistic momentum in the proton rest frame [1]. Hence, within the context of the ordinary space-time description, one can anticipate that the small-x region is dominated by sea-quark and gluon effects arising from the short-distance behavior of QCD, while the behavior at moderate x values could be expected to be determined by the same nonrelativistic interactions of constituent quarks manifested in low energy spectroscopy.

Several previous studies have explored possible connections between low energy properties of the nucleon's quark structure and the inelastic structure functions. Early qualitative discussions of the F_2 structure function ratio and the nucleon spin asymmetry by Close [5] and Carlitz [6] gave compelling symmetry arguments showing that the SU(6) breaking required to explain mass splittings in the baryon ground state should also give agreement with the trends in deep-inelastic observables which violate SU(6). Subsequently, detailed calculations were undertaken by Le Yaouanc and co-workers [7] to explicitly compute the nucleon structure function from a low energy model of the nucleon wave function. Surprisingly, the results were found to qualitatively contradict those of the symmetry arguments of Refs. [5, 6]. However, other detailed calculations of nucleon structure functions by Close and Thomas [8] in the MIT bag model, and by Dziembowski *et al.* [9] in the NRQM, did succeed in relating the spin and flavor deformation of quark parton distributions to the QCD-hyperfine interaction in a low energy model of the nucleon. In this paper we carefully reexamine the rest frame to light-cone connection and the signs of the mixing angles, involved in the calculations, to resolve these discrepancies.

The plan of the paper is as follows. In Sec. II A, the conventional quark model wave function in the nucleon

at rest is discussed. In Sec. II B, quark position-space distributions are calculated which explicitly show the space-spin and space-flavor asymmetries induced by the color hyperfine interactions. The quark-parton model is usually formulated in a reference frame in which the nucleon has a very large momentum ($P_z \to \infty$) or alternatively in terms of new variables corresponding to rotating t and z to the light cone. In Sec. III A we recall the relevance of these light-cone variables for the interpretation of the deep-inelastic scattering data. Then in Sec. III B, the wave function for the nucleon in motion is constructed from the rest frame constituent quark model wave function. The present method is based on earlier work by Susskind [10], Kogut and Soper [11] where systematic use is made of a Lorentz frame in which the nucleon momentum is allowed to approach infinity. As discussed in Sec. III C this systematic procedure avoids the extreme kinematical and weak binding assumptions, implemented in the calculation of Refs. [7, 12]. These assumptions seem to be responsible for the apparent contradiction between the spectroscopic and deep-inelastic scattering evidences for the hyperfine forces of the OGEP type in Ref. [13].

In Sec. III D we use the quark light-cone wave function to compute the longitudinal and transverse momenta distributions of valence partons within the nucleon, which show the momentum-dependent spin and flavor asymmetries induced by the color hyperfine interaction. These distributions provide the reference-scale parton distributions for input to a QCD evolution procedure carried out in Sec. III E. This step introduces gluons and $q\bar{q}$ pairs into the nucleon and completes the connection between the constituent quark wave function and the quark spin and flavor distribution functions measured in experiments. The ratio of spin averaged structure functions for neutron and proton, and the deep-inelastic spin asymmetries are calculated and discussed in Sec. IV. Good agreement with experiment is found, strongly suggesting that the OGEP does incorporate the essential physics of symmetry breaking in baryon structure, both for mass splittings and nucleon structure function ratios.

II. QUARK SPATIAL DISTRIBUTIONS

A. The nucleon wave function in the NCQM

To set a framework for our discussion, we will briefly summarize the essential elements of the NCQM and then show how the model's dynamics leads to pronounced spin and flavor dependences of quark distributions within the nucleon.

With only a few phenomenological parameters and a simple physical picture, the NCQM allows the direct calculations of many hadronic properties, giving a description of electromagnetic, weak and strong couplings, and decay rates accurate at the 10–15% level [14, 15]. Superficially the use of a nonrelativistic model for nucleon structure would appear to be wholly unjustified. However, it has been shown [16] that there is good reason to believe that a nonrelativistic model with weak quark-quark interactions and large constituent quark masses ($\sim$ 350 MeV) is in fact a good (low momentum scale) approximation to the nucleon structure with "nonlinear chiral quarks," in which the chiral symmetry of the underlying QCD Lagrangian is spontaneously broken.

The advantage of the NCQM over the other principal model of nucleon structure (i.e., the bag model [17]), is that the NCQM is a genuine three-body description in which momentum eigenstates (needed for connection with experimental observables) are obtainable in a straightforward way without undue problems from c.m. motion corrections.

The present work employs the low-momentum-scale description of the nucleon ground state in the NCQM developed by Isgur and Karl [4]. The proton and/or neutron contains three nonrelativistic valence quarks of two flavors (uud/ddu) with effective masses $m \simeq M/3$, adjusted to the values of the magnetic moments. The quarks are assumed to be pointlike, spin-1/2 particles. They carry a color quantum number that influences the permutation symmetry of the nucleon wave function.

The model contains two dynamical elements for explaining the nucleon ground-state properties. A nonrelativistic Hamiltonian is split into

$$H = H_{\rm SI} + H_{\rm SD}. \tag{1}$$

The spin-independent part

$$H_{\rm SI} = \sum_i \left(m_i + \frac{\boldsymbol{p}_i^2}{2m_i} \right) + \sum_{i<j} \left(\frac{1}{2} k r_{ij}^2 + U^{ij} \right), \tag{2}$$

includes a confining harmonic potential plus an anharmonicity U^{ij} which together determine the overall size of the system and give a symmetric momentum spread to the three-quark state. On the other hand, the spin-dependent part comprises the contact and tensor spin-spin interactions of the two-body Fermi-Breit potential from the nonrelativistic reduction of one-gluon exchange:

$$H_{\rm SD} = \sum_{i<j} \frac{2\alpha_s}{3m_i m_j} \left\{ \frac{8\pi}{3} \mathbf{S}_i \cdot \mathbf{S}_j \delta^3(\mathbf{r}_{ij}) + \frac{1}{r_{ij}^3} \left[\frac{3(\mathbf{S}_i \cdot \mathbf{r}_{ij})(\mathbf{S}_j \cdot \mathbf{r}_{ij})}{r_{ij}^2} - \mathbf{S}_i \cdot \mathbf{S}_j \right] \right\}, \tag{3}$$

where $\mathbf{r}_{ij} = \mathbf{r}_i - \mathbf{r}_j$, $\mathbf{S}_i$ is the spin of the ith quark, and α_s is the effective quark-gluon coupling constant.

In the Isgur-Karl implementation of the OGEP, the spin-orbit part of the Fermi-Breit potential has been neglected because its inclusion spoiled the agreement with the baryon resonance spectrum. Moreover, the anharmonicity U_{ij} and the QCD-inspired hyperfine Hamiltonian in (3) are treated as a perturbation. A basis of harmonic oscillator wave functions with the same oscillator parameter for each relative coordinate is used to perform perturbation theory calculations.

The short-range contact force in (3) is repulsive for quark pairs in a spin-1 state and attractive for those in a spin-0 state. It is known [3] to make the $\Delta(1232)$ (with spin 3/2) more massive than the nucleon (with spin 1/2). The same force that splits the Δ and nucleon also modifies their wave functions. References [18, 19] estimated

the first order perturbation-theory wave function correction for the nucleon ground state. In general, there are five SU(6) states with $J^P = \frac{1}{2}^+$ up to $\mathcal{N}$=2 that can mix through the hyperfine interaction. Using the notation and conventions of Ref. [19] (summarized in Appendix A of this paper), the nucleon ground state is of the form

$$|N\rangle = \cos\varphi\ |N_S\rangle + \sin\varphi\ |N_M\rangle, \tag{4}$$

where the totally symmetric component $|N_S\rangle$ contains **56** plus **56′** components and is given by

$$|N_S\rangle = \frac{1}{\sqrt{2}}(\chi^\rho\,\varphi^\rho + \chi^\lambda\,\varphi^\lambda)\,(\cos\theta\ \Phi^S + \sin\theta\ \Phi^{S'}), \tag{5}$$

and the mixed-symmetry $|N_M\rangle$ component contains the **70**, $\mathcal{N}$=2 component and is given by

$$|N_M\rangle = \frac{1}{2}(\chi^\rho\,\varphi^\rho\,\Phi^\lambda + \chi^\rho\,\varphi^\lambda\,\Phi^\rho + \chi^\lambda\,\varphi^\rho\,\Phi^\rho - \chi^\lambda\,\varphi^\lambda\,\Phi^\lambda). \tag{6}$$

A small D-wave component [19] has been neglected here.

In Ref. [19], the mixing angles φ and θ appearing in (4) and (5) were fitted to baryon octet spectroscopy with the results

$$\sin\varphi \simeq -0.27 \text{ and } \sin\theta \simeq -0.35. \tag{7}$$

The oscillator parameter value $\alpha = 410$ MeV was used in the fit, with the constituent quark mass value $m = 336$ MeV. It has been shown in Ref. [20] that relativizing the Isgur-Karl model does not substantially change the composition of the physical nucleon state.

In the first published analysis of this problem, the authors of Ref. [18] obtained similar results for the mixing angle φ while neglecting the **56′** component. Note that the sign of the mixing angle φ in (7) is opposite to that of Ref. [18] because we use a different phase convention for the configuration-space wave function in (4). For our phase convention, see Appendix A.

It has been argued on physical grounds [21, 22] that a spatially dependent spin-spin interaction that is, like the one in (3), more repulsive for quarks with parallel rather than antiparallel spins, induces a segregation of charge within the nucleon. This effect leads to a negative mean-square charge radius (MSCR) of the neutron and increases the size of the proton (compared to the size obtained with the unperturbed symmetric wave function only). But it should be noted that the proton and neutron MSCR computed from the valence wave functions of Eq. (4), while in the correct ratio to one another, are incorrect in absolute value by a factor of 3 to 4 [23].

The above observation apparently indicates some imperfections of the NCQM in general and defects of the standard nonrelativistic method of MSCR calculations in particular. The conventional quark model formula for charge radii is based on simple additivity $\langle r^2\rangle = \sum\langle N|e_i\,\mathbf{r}_i^2|N\rangle$. This expression does not take into account that the radii are derived from the electron scattering amplitudes at nonzero momentum transfer q. In particular, the Lorentz boost from P to $P+q$ contributes to both nucleon anomalous magnetic moment and charge radius [24]. This gives nontrivial corrections to calculations based on simple additivity. Studies of these relativistic corrections for the nucleon model of Eq. (4) are in progress and will be reported soon.

The above-mentioned inability of the *harmonic-oscillator* implementation of the NCQM to simultaneously fit spectroscopy and ground-state size has been observed to be corrected (i) by replacing the harmonic-oscillator basis for the nucleon unperturbed states in (4) by a more accurate hyperspherical harmonic expansion technique [25] or/and (ii) by inclusion of the "pion cloud" which arises naturally from spontaneous breaking of chiral symmetry [26, 27]. Alternatively, one could simply fit the harmonic oscillator parameter α and mixing angle to the nucleon size rather than to the baryon octet spectroscopy. This refitting has been shown [28] to permit correct radii to be obtained without affecting the calculated deep-inelastic neutron-to-proton structure function ratio and the nucleon spin asymmetries. These latter corrections are omitted from the present work, which focuses on the results obtainable from the hyperfine configuration mixing. Inclusion of the pionic corrections and more systematic studies of the sensitivity of the presented results for the asymmetries to details of the three-quark wave function will be also examined in the future.

It has been shown previously [28] that the segregation effects for the **56** + **70** mixed wave function, induced by the $\boldsymbol{S}_i \cdot \boldsymbol{S}_j$ term in the hyperfine interaction (3), can be approximated by a diquark cluster wave function. This approximation provides simple physical interpretation of the **56** + **70** mixing. However, the clustering effect is quantitatively rather weak (as noted in Ref. [28]).

B. Quark spatial distributions in the NCQM

Using the nonrelativistic three-body wave functions obtained from the perturbation theory approach outlined above, one can obtain spatial distributions for quarks with different spins and flavors within the nucleon. The distributions are defined by

$$\begin{aligned} q_i^N(r) &= \sum_k \langle N\uparrow|P_{q_i}^{(k)}\ \delta^3(\mathbf{r}-\mathbf{r}_k)|N\uparrow\rangle \\ &= 3\ \langle N\uparrow|P_{q_i}^{(3)}\ \delta^3(\mathbf{r}-\mathbf{r}_3)|N\uparrow\rangle. \end{aligned} \tag{8}$$

Here, $P_{q_i}^{(k)}$ is the projector for the kth quark on the quark with flavor q and spin i.

Within the present model, the proton's distributions can be computed analytically from Eq. (8) and the proton wave function of Eq. (4). The resulting spin-flavor distributions in the proton are given explicitly by

$$\begin{aligned} u_\uparrow(r) = {} & \tfrac{5}{3}\cos^2\varphi\ I_{SS}(r) + \sqrt{2}\ \tfrac{4}{3}\sin\varphi\cos\varphi\ I_{S\lambda}(r) \\ & + \tfrac{1}{2}\sin^2\varphi\ [\tfrac{5}{3}\ I_{\lambda\lambda}(r) + I_{\rho\rho}(r)], \end{aligned} \tag{9a}$$

$$\begin{aligned} u_\downarrow(r) = d_\uparrow(r) = {} & \tfrac{1}{3}\cos^2\varphi\ I_{SS}(r) - \frac{\sqrt{2}}{3}\sin\varphi\cos\varphi\ I_{S\lambda}(r) \\ & + \tfrac{1}{2}\sin^2\varphi\ [\tfrac{1}{3}\ I_{\lambda\lambda}(r) + I_{\rho\rho}(r)], \end{aligned} \tag{9b}$$

$$\begin{aligned} d_\downarrow(r) = {} & \tfrac{2}{3}\cos^2\varphi\ I_{SS}(r) - \sqrt{2}\ \tfrac{2}{3}\sin\varphi\cos\varphi\ I_{S\lambda}(r) \\ & + \tfrac{1}{3}\sin^2\varphi\ I_{\lambda\lambda}(r). \end{aligned} \tag{9c}$$

The overlap integrals for states $(SS, S\lambda, \lambda\lambda, \rho\rho)$ are defined in Appendix B. The distributions of Eq. (9) are plotted in Fig. 1 for the full wave function of Ref. [19], which has the mixing angles given in (7) and contains **56** + **56′** + **70** components. The **56′** component has been neglected in some previous works on the present subject [7, 9], essentially because it is itself SU(6) symmetric and so would not be expected to contribute to SU(6)-breaking asymmetries in the quark distributions.

In a totally symmetric nucleon model ($\varphi = \theta = 0$), all of the distributions given above would be proportional to one another according to

$$u_\uparrow(r) = \tfrac{5}{3} f(r), \quad u_\downarrow(r) = d_\uparrow(r) = \tfrac{1}{3} f(r), \quad d_\downarrow(r) = \tfrac{2}{3} f(r), \tag{10}$$

where $f(r)$ is a Gaussian function given in Appendix B. The symmetric limit is indicated in Fig. 1 by the dashed curve for $u_\uparrow(r)$.

Several observations should be made about the distributions shown in Fig. 1. Note that in Eq. (9b) we still have $u_\downarrow(r) = d_\uparrow(r)$. Also, the constituent quarks are seen to be highly polarized $(u_\uparrow(r) \gg u_\downarrow(r), d_\downarrow(r))$. This would of course be true in the symmetric limit as well, due essentially to the overall bound state quantum numbers.

The novel effect of the color hyperfine interaction (3) is to shift $u_\downarrow(r) = d_\uparrow(r)$ and $d_\downarrow(r)$ components slightly to smaller r leaving at large r the dominant $u_\uparrow(r)$ distribution. This flavor-spin asymmetry is more pronounced when the **56′** component is neglected. This result could have been anticipated from the argument given in Ref. [7] for neglect of the **56′** component. The flavor-spin asymmetry will survive when transformed to light-cone momentum space, where it shows up as SU(6)-violating x dependence of structure function ratios and spin asymmetries.

III. QUARK MOMENTUM DISTRIBUTIONS

A. Structure functions and light-cone dynamics

The deep inelastic electron- (or muon-)nucleon cross section is determined by the hadronic tensor

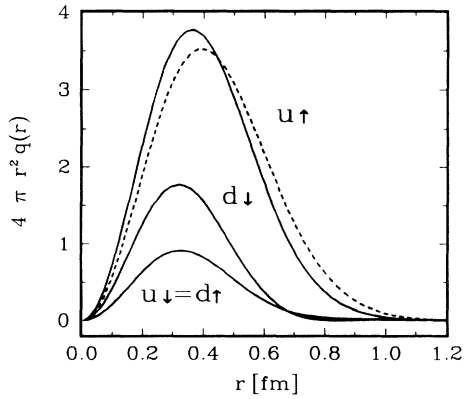

FIG. 1. The quark spatial distributions $q(r)$ for the **56** + **56′** + **70** mixing.

$W_{\mu\nu}(q, P, S)$, where q is the virtual photon momentum ($q^2 \equiv -Q^2$), P and S are the nucleon momentum and polarization, respectively. The hadronic tensor is a current-current correlation function

$$W_{\mu\nu}(q, P, S) = \frac{1}{8\pi} \int d^4\xi \; e^{iq\cdot\xi} \langle N(P,S)| J^{\rm em}_\mu(\xi) J^{\rm em}_\nu(0) |N(P,S)\rangle. \tag{11}$$

It depends on the electromagnetic current density, $J^{\rm em}_\mu(\xi)$ and the physical nucleon state $|N(P,S)\rangle$, represented by a wave function that is an eigenfunction of momentum, energy, and spin. Changing variables for any four vector from the ordinary time-space components $a = (a_0, a_z, \mathbf{a}_\perp)$ to *light-cone* variables $a = (a^+, a^-, \mathbf{a}_\perp)$, where $a^\pm = a_0 \pm a_z$ one can show [29] that in the Bjorken limit of deep-inelastic scattering (DIS) (i.e., $q^- \to \infty, q^+$ fixed) the integrand in (11) is dominated by contributions from the tangent plane to the light-cone $\xi^+ = 0$. Thus the appropriate form of relativistic dynamics [30, 31] for the description of DIS is not the instant form but rather the light-cone form with the coordinate ξ^+ treated as a "time" coordinate. Then, with this choice of dynamics the current-current correlation function in (11) becomes a *static* correlation function determined exclusively by the nucleon light-cone wave function [32, 33].

B. The nucleon wave function on the light cone

If we let the variable ξ^+ play the role of time and quantize QCD on the null plane, then a nucleon can be described by the Fock space expansion

$$|N\rangle = \Psi^N_{qqq}|qqq\rangle + \Psi^N_{qqqg}|qqqg\rangle + \Psi^N_{qqqq\bar{q}}|qqqq\bar{q}\rangle + \cdots, \tag{12}$$

where the first valence term contains only three quarks but the other terms include gluons and quark-antiquark pairs. The coefficients

$$\Psi^N(x_1, \mathbf{p}_{\perp 1}, \lambda_1, \ldots), \tag{13}$$

in this light-cone Fock expansion are the parton wave functions which depend on the light-cone constituent momentum variables x_i and $\mathbf{p}_{\perp i}$, as well as on helicity λ_i and other internal variables of the ith parton.

The variable x_i is defined as a fraction of the plus component of the nucleon momentum carried by the parton, so that $p^+_i = x_i P^+$. Values of x_i must lie in the range [0,1]. The light-cone momentum coordinates x_i with $(\sum x_i = 1)$ and $\mathbf{p}_{\perp i}$ with $(\sum \mathbf{p}_{\perp i} = 0)$, respectively, are actually relative coordinates, i.e., they are independent of the total momentum P^+ and $\mathbf{P}_\perp$ of the nucleon.

As shown by Leutwyler and Stern in Ref. [31], the light-cone wave function Ψ is invariant under all kinematical Poincaré group generators, including a Lorentz boost along the z direction. Hence, it is determined if it is known at the nucleon rest frame. This feature brings great simplification to model building as well as matrix element calculations where the nucleon wave function in

different frames is required as an input.

The NCQM is based on the hypothesis that hadrons may be approximately described in terms of rest-frame configurations of a definite number of quarks and antiquarks. Although this so-called *valence*-quark approximation has not been derived from any underlying field theory of strong interactions, it is usually formulated in a language of the instant-form Fock-space representation. For instance, a nucleon state is approximated in this framework by

$$|N\rangle \approx \int \prod d^3\mathbf{p}\, \Psi^N(\mathbf{p}_1,\lambda_1,\mathbf{p}_2,\lambda_2,\mathbf{p}_3,\lambda_3)\, b^\dagger_{\mathbf{p}_1\lambda_1} b^\dagger_{\mathbf{p}_2\lambda_2} b^\dagger_{\mathbf{p}_3\lambda_3} |0\rangle, \tag{14}$$

where Ψ^N is taken to be the nucleon rest frame wave function, a solution of the Schrödinger equation. The indices other than momentum and spin have been suppressed.

Since the work by Weinberg [34] it is known that a Fock state description of bound states is only well defined in the infinite-momentum frame (IMF) of the instant-form dynamics, due to the simplified vacuum structure in this limit. Later, Susskind [10] showed that the IMF limiting procedure is essentially a change of variables from the laboratory time and z coordinates (ξ_0,ξ_z) to the light-cone time and space coordinate (ξ^+,ξ^-). We shall use here Susskind's method to connect the quark momenta and spins in (14) to the light-cone counterparts in (13).

In the IMF limit the observer is supposed to be moving, with respect to the nucleon-rest frame, at high velocity in the negative z direction. Hence for a quark with momentum $\mathbf{k}$ and energy k_0 in the fast moving frame where the nucleon has energy E and the momentum along the z axis P, the quark momenta in the nucleon rest frame are given by the inverse Lorentz boost $p = L(p \leftarrow k)\,k$, i.e.,

$$\begin{aligned} p_0 &= \cosh\omega\, k_0 - \sinh\omega\, k_z, \\ p_z &= \cosh\omega\, k_z - \sinh\omega\, k_0, \\ \mathbf{p}_\perp &= \mathbf{k}_\perp, \end{aligned} \tag{15}$$

where

$$\cosh\omega = \frac{E}{M}, \quad \sinh\omega = \frac{P}{M}. \tag{16}$$

Expressing the longitudinal momentum of a quark in the fast moving frame in terms of a fraction η,

$$k_z = \eta P \ \text{ with } \ \sum \eta = 1, \tag{17}$$

and letting $P \to \infty$, with the η held fixed and *positive*, one gets, for the quark on-shell energy,

$$\begin{aligned} k_0 &= \sqrt{\eta^2 P^2 + \mathbf{k}_\perp^2 + m^2} \\ &= \eta P + \frac{\mathbf{k}_\perp^2 + m^2}{2\eta P} + O(P^{-2}), \end{aligned} \tag{18}$$

and, for nucleon energy,

$$E = \sqrt{P^2 + M^2} = P + \frac{M^2}{2P} + O(P^{-2}), \tag{19}$$

respectively. Now if these relations are used in Eq. (15), for

$$p = \lim_{P\to\infty} L(p \leftarrow k)\,k, \tag{20}$$

then all infinities cancel out consistently and a finite limit is obtained:

$$\begin{aligned} p_0 &= \frac{1}{2}\left(\eta M + \frac{\mathbf{p}_\perp^2 + m^2}{\eta M}\right), \\ p_z &= \frac{1}{2}\left(\eta M - \frac{\mathbf{p}_\perp^2 + m^2}{\eta M}\right), \\ \mathbf{p}_\perp &= \mathbf{k}_\perp. \end{aligned} \tag{21}$$

Thus the limiting Lorentz boost indicated by (20) in fact gives a definite and finite result relating rest frame momenta p to IMF variables $(\eta,\mathbf{p}_\perp)$. Now, identifying in the IMF, the longitudinal fraction $\eta = k_z/P$ and the light cone fraction $x = k^+/P^+$, one finds that the finite limit of the Lorentz boost in Eq. (21) is essentially a *change of variables* from the ordinary quark momentum (p_0,p_z) to the light-cone momentum (p^-,p^+) or equivalently the longitudinal momentum fraction and the transverse momentum $(x,\mathbf{p}_\perp)$, i.e.,

$$p_0 = \frac{1}{2}(p^+ + p^-) = \frac{1}{2}\left(xM + \frac{\mathbf{p}_\perp^2 + m^2}{xM}\right), \tag{22}$$

$$p_z = \frac{1}{2}(p^+ - p^-) = \frac{1}{2}\left(xM - \frac{\mathbf{p}_\perp^2 + m^2}{xM}\right), \tag{23}$$

$$\mathbf{p}_\perp = \mathbf{k}_\perp. \tag{24}$$

The above IMF boost or the equivalent change of momentum variables in Eqs. (22) and (23) requires a corresponding change of spin basis. As is known from Ref. [35], the ordinary spin basis $|\mathbf{p},s\rangle_T$ of the instant-form dynamics is related to a spin basis $|p^+,\mathbf{p}_\perp,s\rangle$ of the light-cone dynamics by a certain rotation in spin space. For a spin-1/2 particle the rotation is known as the Melosh transformation [36]. Although the Melosh rotation $\mathcal{R}$ which gives $|\mathbf{p},s\rangle_T = \sum \mathcal{R}_{s's}|p^+,\mathbf{p}_\perp,s'\rangle$, is derived in Ref. [35] we rederive the connection here by direct boosting of the Dirac spinors to IMF. This parallels the derivation of Eqs. (22) and (23) demonstrating a systematic feature of the method.

For a free quark with momentum $\mathbf{k}$ in the fast moving frame and with spin projection s along the z axis, the Dirac spinor in the standard representation [37] has the form

$$u(\mathbf{k},s) = [k_0+m]^{1/2}\begin{pmatrix} \chi(s) \\ \dfrac{\boldsymbol{\sigma}\cdot\mathbf{k}}{k_0+m}\,\chi(s) \end{pmatrix}, \tag{25}$$

where the Pauli spinors are

$$\chi(\uparrow) = \begin{pmatrix}1\\0\end{pmatrix}, \quad \chi(\downarrow) = \begin{pmatrix}0\\1\end{pmatrix}. \tag{26}$$

Using the spinor representation of the boost operator $p = L(p \leftarrow k)\, k$ in Eq. (15),

$$S(p \leftarrow k) = \cosh \frac{\omega}{2} - \alpha_z \sinh \frac{\omega}{2}, \tag{27}$$

and defining

$$\mathcal{U}(p^+, \mathbf{p}_\perp, s) = \lim_{P \to \infty} S(p \leftarrow k)\, u(\mathbf{k}, s), \tag{28}$$

the infinite momentum spinors of Ref. [38] are obtained:

$$\mathcal{U}(p^+, \mathbf{p}_\perp, s)$$

$$= \frac{1}{\sqrt{2p^+}} \begin{pmatrix} (p^+ + m)\, \chi(s) + \boldsymbol{\sigma}_\perp \cdot \mathbf{p}_\perp\, \sigma_z\, \chi(s) \\ (p^+ - m)\, \sigma_z\, \chi(s) + \boldsymbol{\sigma}_\perp \cdot \mathbf{p}_\perp\, \chi(s) \end{pmatrix}. \tag{29}$$

Substituting $\chi(s)$ from Eq. (26) gives the final result

$$\mathcal{U}(p^+, \mathbf{p}_\perp, \uparrow) = \frac{1}{\sqrt{2p^+}} \begin{pmatrix} p^+ + m \\ p^R \\ p^+ - m \\ p^R \end{pmatrix},$$

$$\mathcal{U}(p^+, \mathbf{p}_\perp, \downarrow) = \frac{1}{\sqrt{2p^+}} \begin{pmatrix} -p^L \\ p^+ + m \\ p^L \\ -p^+ + m \end{pmatrix}, \tag{30}$$

where $p^{L,R} = p_x \mp i p_y$, and $p^+ = x\, M$.

It can be shown [39] that the conventional Dirac spinors of Eq. (25) are connected to the IMF spinors of Eq. (29) or Eq. (30) by the Melosh rotation

$$u(\mathbf{p}, s) = \sum \mathcal{R}_{s's}\, \mathcal{U}(p^+, \mathbf{p}_\perp, s'), \tag{31}$$

where the matrix elements of $\mathcal{R}$ are given by

$$u(\mathbf{p}, \uparrow) = N^{-1}(x, \mathbf{p}_\perp)\, [\,(p^+ + m)\, \mathcal{U}(p^+, \mathbf{p}_\perp, \uparrow) - p^R\, \mathcal{U}(p^+, \mathbf{p}_\perp, \downarrow)], \tag{32a}$$

$$u(\mathbf{p}, \downarrow) = N^{-1}(x, \mathbf{p}_\perp)\, [\,(p^+ + m)\, \mathcal{U}(p^+, \mathbf{p}_\perp, \downarrow) + p^L\, \mathcal{U}(p^+, \mathbf{p}_\perp, \uparrow)], \tag{32b}$$

with the normalization

$$N(x, \mathbf{p}_\perp) = \sqrt{2p^+\,(p_0 + m)}. \tag{33}$$

Returning to the construction of the light-cone wave function, we are now in possession of all the elements necessary to write down the momentum and spin part of the wave function. The Schrödinger wave functions given in Eqs. (A15)–(A18) are transformed by applying the substitution of Eqs. (23) and (24) and multiplying by a factor $N_i\, (\prod x_i)^{-1/2}$, defining at last the light-cone momentum space wave function:

$$\Phi^i_{\mathrm{LC}}(x_1, x_2, x_3, \mathbf{p}_{\perp 1}, \mathbf{p}_{\perp 2}, \mathbf{p}_{\perp 3})$$

$$= N_i\, \Phi^i(\mathbf{p}_1, \mathbf{p}_2, \mathbf{p}_3)/\sqrt{x_1 x_2 x_3}. \tag{34}$$

The index i refers to the wave function components with different symmetries (S, S', ρ, λ) given in Appendix A. The coefficients N_i are determined by imposing the conventional light-cone normalization condition [40]

$$\int [dx]\, [d^2 p_\perp]\, |\Phi_{\mathrm{LC}}(x_i, \mathbf{p}_{\perp i})|^2 = 1, \tag{35}$$

where $[dx] = \prod dx\ \delta(\sum x - 1)$ and $[d^2 p_\perp] = \prod d^2 \mathbf{p}_\perp\ \delta(\sum \mathbf{p}_\perp)$. It should be noted that the standard light-cone measure factor $1/\prod x_i$ was absorbed into the function in (34).

With the Melosh rotation of Eq. (31), the light-cone spin wave functions for the ρ and λ wave function components in (5) and (6) are given by

$$\chi^i_{\mathrm{LC}} = \mathcal{R}_1 \otimes \mathcal{R}_2 \otimes \mathcal{R}_3\, \chi^i. \tag{36}$$

The light-cone spin wave functions resulting from this transformation are given in Tables I and II.

With these results, the rest frame wave function of the conventional constituent quark model is now transformed into a valence component of the light-cone wave function.

As described, the underlying nucleon model contains four parameters: the Gaussian spread α, the quark constituent mass m, and the mixing angles θ and φ. We keep these parameters fixed at the values obtained from fits to baryon spectroscopy in (7). Augmented by the transformations just discussed, high energy nucleon structure can also be investigated with the same underlying model.

C. Discussion of related work

Before proceeding with the calculation of deep-inelastic scattering observables, some limiting cases of Eqs. (22) and (23) will be discussed in order to make connections with earlier work [7, 41, 42].

Note first that expanding $p_0 = \sqrt{m^2 + \mathbf{p}^2}$ on the left-hand side (LHS) of Eq. (22) through terms quadratic in momentum and summing over the three constituent particles gives the Brodsky-Huang-Lepage prescription [43]

$$2M \left(M - 3m - \sum \frac{\mathbf{p}^2}{2m}\right) \simeq M^2 - M_0^2, \tag{37}$$

where

$$M_0^2 = \sum \frac{\mathbf{p}_\perp^2 + m^2}{x}. \tag{38}$$

This prescription has been used in various collaborative

TABLE I. The light-cone spin wave function $\chi^\rho_\uparrow$ with $a = x\, M + m$, $p^{L,R} = p_x \mp i\, p_y$, and N given in Eq. (33).

$\lambda_1\ \lambda_2\ \lambda_3$	$\chi^\rho_\uparrow \times \sqrt{2}\ N_1 N_2 N_3$
$\uparrow\uparrow\uparrow$	$a_1\, a_3\, p_2^L - a_2\, a_3\, p_1^L$
$\uparrow\uparrow\downarrow$	$a_2\, p_1^L\, p_3^R - a_1\, p_2^L\, p_3^R$
$\uparrow\downarrow\uparrow$	$a_1\, a_2\, a_3 + a_3\, p_1^L\, p_2^R$
$\uparrow\downarrow\downarrow$	$-a_1\, a_2\, p_3^R - p_1^L\, p_2^R\, p_3^R$
$\downarrow\uparrow\uparrow$	$-a_1\, a_2\, a_3 - a_3\, p_1^R\, p_2^L$
$\downarrow\uparrow\downarrow$	$a_1\, a_2\, p_3^R + p_1^R\, p_2^L\, p_3^R$
$\downarrow\downarrow\uparrow$	$a_1\, a_3\, p_2^R - a_2\, a_3\, p_1^R$
$\downarrow\downarrow\downarrow$	$a_2\, p_1^R\, p_3^R - a_1\, p_2^R\, p_3^R$

TABLE II. The light-cone spin wave function $\chi^\lambda_\uparrow$ with $a = x\,M + m, p^{L,R} = p_x \mp i\,p_y$, and N given in Eq. (33).

$\lambda_1\ \lambda_2\ \lambda_3$	$\chi^\lambda_\uparrow\ \sqrt{6}\ N_1 N_2 N_3$
$\uparrow\uparrow\uparrow$	$2a_1\ a_2\ p_3^L - a_1\ a_3\ p_2^L - a_2\ a_3\ p_1^L$
$\uparrow\uparrow\downarrow$	$2a_1\ a_2\ a_3 + a_1\ p_2^L\ p_3^R + a_2\ p_1^L\ p_3^R$
$\uparrow\downarrow\uparrow$	$-a_1\ a_2\ a_3 - 2\ a_1\ p_2^R\ p_3^L + a_3\ p_1^L\ p_2^R$
$\uparrow\downarrow\downarrow$	$a_1\ a_2\ p_3^R - p_1^L\ p_2^R\ p_3^R - 2\ a_1\ a_3\ p_2^R$
$\downarrow\uparrow\uparrow$	$-a_1\ a_2\ a_3 - 2\ a_2\ p_1^R\ p_3^L + a_3\ p_1^R\ p_2^L$
$\downarrow\uparrow\downarrow$	$a_1\ a_2\ p_3^R - p_1^R\ p_2^L\ p_3^R - 2\ a_2\ a_3\ p_1^R$
$\downarrow\downarrow\uparrow$	$2\ p_1^R\ p_2^R\ p_3^L + a_1\ a_3\ p_2^R + a_2\ a_3\ p_1^R$
$\downarrow\downarrow\downarrow$	$2a_3\ p_1^R\ p_2^R - a_1\ p_2^R\ p_3^R - a_2\ p_1^R\ p_3^R$

works by one of the present authors [44] and also by others [45, 46].

If we use the additional approximation $m \simeq M/3$ (this is often referred to in the literature as the weak binding approximation), put $\mathbf{p}_\perp = 0$, and expand the right-hand side (RHS) of Eq. (23) to lowest nonvanishing order in $(x - 1/3)$, we obtain

$$p_z \simeq M\,(x - 1/3). \tag{39}$$

This limit of Eq. (23) is referred to in Ref. [7] as the Licht-Pagnamenta prescription. Extensive use has been made of this expression [7] as a mapping from p_z to x over the entire kinematic range of p_z from $-\infty$ to $+\infty$. However, applying this prescription away from $x \sim 1/3$ (i.e., $p_z \sim 0$) is seen to violate the assumptions used in its derivation. This leads to a number of technical and qualitative problems, including improper support properties in x for the light-cone quark distributions, and to structure function ratios with qualitatively different x dependences than those resulting from use of the full Eq. (23) (see below). It should be noted that the IMF spinor of Eq. (29) also disagrees with the corresponding spinors used in Refs. [7, 47].

The transformation given in (23) and (24) on the other hand has a number of desirable features. It is kinematically relativistic and reduces to the Licht-Pagnamenta prescription when $p_\perp \to 0$ and $x \to 1/3$. Equation (23) also has reasonable behavior at the end points of the allowed interval in x. For a fixed $p_\perp$ and $x \to 0$ it gives $p_z \to \infty$ in accordance with the definition of the light-cone fraction x, where the limit $x \to 0$ implies very large constituent momentum in the nucleon rest frame [1]. On the other hand, for $x \to 1$ Eq. (23) gives a finite, moderately relativistic value for p_z. As will be seen below, Eq. (23) also leads to results for the structure function ratios which are in good agreement with experiment, while using the symmetry breaking parameter values fitted to baryon mass splittings.

Other alternatives to the present procedure also exist. Recently Coester and others [48] used Eqs. (22) and (23) for transformation of momenta to the light cone, but replaced M by M_0 throughout. This permitted a unitary relation to be obtained between the wave function expressed in the center-of-mass momenta and light-cone variables. It also guaranteed that constraints such as $\Sigma p_z = 0$ remained valid when expressed in terms of light-cone variables. Unfortunately we have found that this appealing approach gives physically unreasonable results, for example that the proton structure function at large x is dominated by down quarks rather than up. Another option is to apply Eqs. (23) and (24) as given above to the momentum wave function written in terms of relative momenta Eqs. (A11)–(A14) and obtain a unitary transformation of the wave function to ligh-cone variables. We find that this procedure also leads to incorrect structure functions with, for example, the proton dominated by down quarks at large x.

The normalization of Tables I and II is different from that given in Ref. [42] and later used in Refs. [44, 45]. In the previous work, the normalization coefficient of the Melosh transformation $N(x, \mathbf{p}_\perp) = \sqrt{2p^+\,(p_0 + m)}$ had to be approximated by $\sqrt{2x\,P^+\,(2\,m)}$, because the technical facility for performing multidimensional integration with respect to the $\mathbf{p}_\perp$ variable was lacking. The normalization given in the present work is more accurate since the full multidimensional integration can now be performed, including the kinematical dependence of the $N(x, \mathbf{p}_\perp)$. For this task the VEGAS algorithm invented by Lepage [49] has been used, along with the very efficient routine FDAI by Dydek and Pindor [50]. All symbolic calculations for this work have been developed in MATHEMATICA [51].

D. Quark light-cone momentum distributions

Quark probability distributions derived from the IMF or light-cone Fock expansion are of the form [32, 33]

$$\begin{aligned} q_i^N(x, \mathbf{p}_\perp) &= \sum_l \langle N \uparrow | P_{q_i}^{(l)}\ \delta(x - x_l)\ \delta^2(\mathbf{p}_\perp - \mathbf{p}_{\perp l}) | N \uparrow \rangle \\ &= 3\ \langle N \uparrow | P_{q_i}^{(3)}\ \delta(x - x_3)\ \delta^2(\mathbf{p}_\perp - \mathbf{p}_{\perp 3}) | N \uparrow \rangle. \end{aligned} \tag{40}$$

Using the explicit form of the light-cone wave function found above, one obtains the following expression for such probability distributions:

$$\begin{aligned} q_i(x, \mathbf{p}_\perp) = {} & \cos^2\varphi\ \mathcal{M}_i^{SS}(x, \mathbf{p}_\perp)\ I_{SS}(x, \mathbf{p}_\perp) + \sin\varphi\ \cos\varphi\ \mathcal{M}_i^{S\lambda}(x, \mathbf{p}_\perp)\ I_{S\lambda}(x, \mathbf{p}_\perp) \\ & + \tfrac{1}{2}\sin^2\varphi\ [\mathcal{M}_i^{SS}(x, \mathbf{p}_\perp)\ I_{\lambda\lambda}(x, \mathbf{p}_\perp) + \mathcal{M}_i^{\rho\rho}(x, \mathbf{p}_\perp)\ I_{\rho\rho}(x, \mathbf{p}_\perp)]. \end{aligned} \tag{41}$$

Note that $\mathcal{M}_i^{SS} = \mathcal{M}_i^{\lambda\lambda}$ for all spin projections i. The factors $\mathcal{M}$ result from the Melosh transformation and are given in Tables III, IV, and V. Their static limits correspond to the spin factors appearing in Eq. (9). The momentum space overlap integrals I_{ij} are explicitly given by

$$\begin{aligned} I_{ij}(x, \mathbf{p}_\perp) = {} & \int [dx][d^2p_\perp]\ \Phi^i_{LC}(x, \mathbf{p}_\perp)\ \Phi^j_{LC}(x, \mathbf{p}_\perp) \\ & \times \delta(x - x_3)\ \delta^2(\mathbf{p}_\perp - \mathbf{p}_{\perp 3}). \end{aligned} \tag{42}$$

TABLE III. Melosh factor $M^{SS}(a^2 + \mathbf{p}_\perp^2)$ with $a = x\,M + m$.

Flavor\spin	↑	↓
u	$(5\,a^2 + \mathbf{p}_\perp^2)/3$	$(a^2 + 5\,\mathbf{p}_\perp^2)/3$
d	$(a^2 + 2\,\mathbf{p}_\perp^2)/3$	$(2\,a^2 + \mathbf{p}_\perp^2)/3$

These multidimensional integrals must be accurately evaluated in order to compute the observables discussed below. The evaluation employs the light-cone relative momenta introduced by Berestetskiĭ-Terent'ev [40] and the numerical method mentioned above.

Structure functions are defined in terms of quark distributions with the $\mathbf{p}_\perp$ dependence integrated out:

$$q_i(x) = \int d^2p_\perp\; q_i(x, \mathbf{p}_\perp). \tag{43}$$

The spin- and flavor-dependent quark distributions $u_i(x, Q_0^2)$ and $d_i(x, Q_0^2)$ for $i = \uparrow, \downarrow$ resulting from this procedure are shown in Fig. 2 for the **56** + **56′** + **70** wave function. Anticipating the results of the next section we introduce the parameter Q_0^2, representing the (unknown) low momentum transfer scale at which these distributions (obtained directly from the nonrelativistic wave function) are expected to represent the nucleon structure. The subtle peak shifts and width differences among the distributions exhibited in Fig. 2 result entirely from the SU(6) breaking inherent in the underlying nucleon model. This is clear since in the static, SU(6)-symmetric model all distributions are proportional to the single universal function of x indicated by the dashed line.

The effect of using the kinematic transformation of Eqs. (23) and (24) is indicated in Fig. 3. The figure contrasts spin averaged quark distributions $u(x)/2$ and $d(x)$ for the proton, calculated with the Licht-Pagnamenta prescription of Eq. (39), with those calculated using Eqs. (23) and (24). Use of Eq. (39) leads to a non-negligible fraction of the distributions lying outside the kinematically allowed region $x \in [0, 1]$. Also, at large x, $d(x)$ is *larger* than $u(x)/2$ when Eq. (39) is used, rather than being smaller as found experimentally and as obtained using Eq. (23). This difference in the quark distribution functions is precisely the reason for the difference in x dependence of the structure function ratios between the present work and Ref. [7]. The apparent contradiction between SU(6)-violating baryon mass splittings and deep-inelastic observables is due to the use of the more approximate Eq. (39) rather than Eq. (23).

The light-cone momentum wave functions given above in Eqs. (34) and (36), combined with Eq. (41), give a full description of the longitudinal *and transverse* momentum

TABLE IV. Melosh factor $M^{S\lambda}(a^2 + \mathbf{p}_\perp^2)$ with $a = x\,M + m$.

Flavor\spin	↑	↓
u	$\sqrt{2}\,(4\,a^2 - \mathbf{p}_\perp^2)/3$	$\sqrt{2}\,(-a^2 + 4\,\mathbf{p}_\perp^2)/3$
d	$-\sqrt{2}\,(a^2 + 2\,\mathbf{p}_\perp^2)/3$	$-\sqrt{2}\,(2\,a^2 + \mathbf{p}_\perp^2)/3$

TABLE V. Melosh factor $M^{\rho\rho}(a^2+\mathbf{p}_\perp^2)$ with $a = x\,M+m$.

Flavor\spin	↑	↓
u	$a^2 + \mathbf{p}_\perp^2$	$a^2 + \mathbf{p}_\perp^2$
d	a^2	$\mathbf{p}_\perp^2$

distributions of quarks within the context of the NCQM. The distributions in the longitudinal momentum fraction x and transverse momentum $\mathbf{p}_\perp$ are not factorizable, and furthermore depend on flavor and spin. The distributions of $\langle p_\perp^2 \rangle$ as a function of x is given by

$$\langle p_\perp^2(x)\rangle_i = \frac{\int p_\perp^2\; d^2p_\perp\; q_i(x, \mathbf{p}_\perp)}{q_i(x)}. \tag{44}$$

The x dependence of $\langle p_\perp(x)\rangle/M^2$ in the NCQM is exhibited in Fig. 4 for u and d flavors separately. Note that the mean square value of $p_\perp^2$ vanishes at $x = 0$ and $x = 1$ as it must on kinematical grounds [52]. In addition the mean square value of the transverse momentum of a d quark at moderate x is calculated to be as much as 30% larger than that of a u quark.

The observed flavor dependence of $\langle p_\perp^2 \rangle$ is as expected from the repulsive OGEP interaction between identical quarks. This causes the u quarks to be more spread-out in coordinate space than the d quarks and therefore to have lower $\langle p_\perp^2 \rangle$. The longitudinal distributions of Fig. 2 *do not* show this intuitive behavior, due to effects of the transformation to the IMF. The counterintuitive behavior of longitudinal distributions has been previously noted by Isgur [22] in the context of the IMF approach.

E. QCD evolution

Before using the present model to compute deep-inelastic observables, the relation between the quarks of light-cone field theory, and the constituent quarks of the NCQM must finally be faced. This is a thorny theoretical problem with no definitive resolution at present. However, detailed model calculations have shown that an empirical connection can be established.

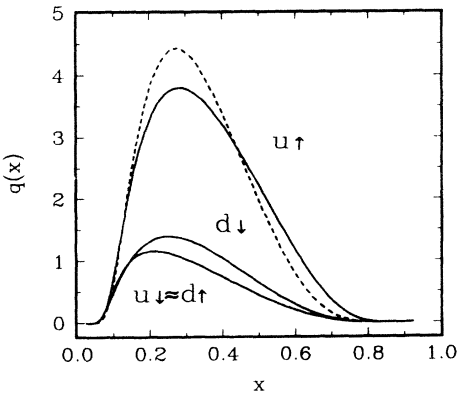

FIG. 2. The quark longitudinal-momentum distributions $q(x)$ for the **56** + **56′** + **70** mixing.

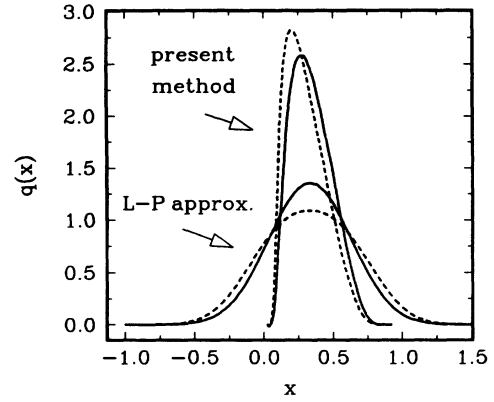

FIG. 3. The spin-averaged quark distributions $q(x)$ obtained with two different transformations of Eqs. (23) and (39); solid line—$u/2$ and dashed line—d quark.

Working in the MIT version of the bag model, Jaffe and Ross [53] proposed that experimental observables should be compared to distributions calculated in the bag model only after these are QCD evolved to some appropriate momentum scale. The experimental momentum transfer dependences of structure function moment ratios were shown to extrapolate at low Q^2 to the values computed in the bag model. The individual moments (except possibly N=2) were shown to be reasonably consistent with a single low scale Q_0^2 being associated with moments from a bag-model calculation, although an accurate value of this scale could not be determined. A similar procedure has been adopted by other bag-model practitioners [54].

In the present work it is proposed to approximate the measured parton-quark and gluon distribution functions by applying QCD evolution to the valencelike input from the nucleon model transformed to the light cone/IMF. It will be shown that in the valence region ($0.2 < x < 0.8$) the resulting structure function ratios and spin asymmetries are in fact not qualitatively changed by the evolution procedure. The main features of the predicted distributions in this region are determined by the underlying spin and flavor dependent OGEP forces in our model.

The technical approach to QCD evolution adopted here is based on the lowest order approach derived by Gribov, Lipatov, Altarelli, and Parisi equations [55]. These equations are of the form

$$\frac{dq(x,t')}{dt'} = \frac{\alpha_s(t')}{2\pi}\int_x^1 \frac{dy}{y} P\left(\frac{x}{y}\right) q(y,t'), \tag{45}$$

where P is a probability function for a quark (or gluon) to split into a quark (or a gluon). The parameter t' appearing in Eq. (45) is given by

$$t' = \frac{2}{\beta_0}\ln\{\alpha_s(Q_0^2)/\alpha_s(Q^2)\}, \tag{46}$$

with $\beta_0 = 11 - 2n_f/3 = 25/3$, for four flavors, and

$$\frac{\alpha_s(Q^2)}{2\pi} = \frac{2}{\beta_0}\frac{1}{\ln(Q^2/\Lambda^2_{\rm QCD})}. \tag{47}$$

In the range $0.03 \le x \le 0.7$ these equations are accurately solvable by the polynomial expansion method of Kumano and Londergan [56]. For $x > 0.7$, the convolution method of Ref. [57] is used to provide improved convergence. Even this method does not allow reliable calculation of structure functions or ratios to the $x = 1$ limit. First, the Gaussian wave functions used here are so strongly cut off at large momenta that numerical accuracy in the unevolved distributions becomes a severe problem above $x = 0.9$. Since the convolution method requires integrals over x, evolved distributions can only be calculated reliably up to $x \simeq 0.85$. Therefore structure function ratio plots are given only for $x < 0.85$ in Sec. IV.

The value of t' is related to the low momentum scale Q_0^2 associated with the unevolved input distributions. In the present work an optimum value 0.55 was obtained by computing the structure function F_2^p and varying t' until the evolved F_2^p matched experimental data (taken from Table 1 of Ref. [58]) near $x = 1/3$ for $Q^2 = 11.5$ GeV^2. For the calculation we have used four active flavors and $\Lambda_{\rm QCD} = 200$ MeV. The value of t' so obtained corresponds to $Q_0 = 266$ MeV. This is of course so small a scale that the use of perturbative QCD evolution is highly suspect. Moreover the detailed x dependence of the predicted F_2^p turns out to be too steep at all x values. This is always the case when pure valence quark inputs are evolved to force a match to experimental structure functions [59]. Adding a small intrinsic sea quark and gluon component to the wave functions has been shown to permit use of a more realistic Q_0. This would also lead to less steep x dependence. In the present work we do not intend to go beyond the conventional NCQM and restrict our prediction to the valence region (conventionally defined [14] as $x > 0.2$). Note that we are interested here in understanding the pattern of symmetry breaking from the conventional NCQM. We show explicitly in Sec. IV that the structure function ratios are actually quite insensitive to the evolution procedure.

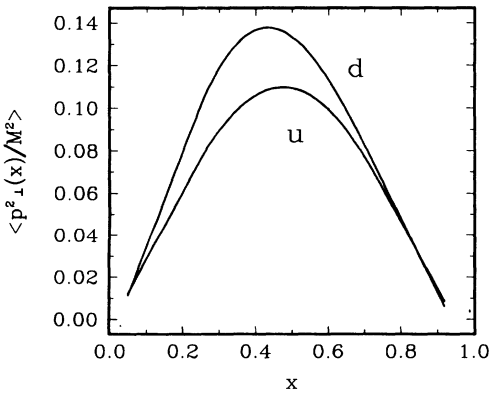

FIG. 4. The quark transverse-momentum distributions $\langle p_\perp^2(x)\rangle$.

IV. RESULTS FOR LONGITUDINAL STRUCTURE FUNCTION RATIOS

The structure functions F_1, g_1, and the spin asymmetry A_1 are defined in the standard way according to for-

mulas given in Appendix C. Figures 5–7 give the results of the present model for the F_1 structure function ratio R^{np} and spin asymmetries $A_1^{p,n}$. The short-dashed lines give the symmetric limit ($\varphi = \theta = 0$), the dot-dashed lines give the result without any QCD evolution, while the solid lines include this effect. Results are given separately for the full **56** + **56′** + **70** wave function and for the restricted **56** + **70** case. The data points and associated errors for the F_1 ratio are from the New Muon Collaboration (NMC) [60], the proton spin asymmetry data are from [61, 62], and the neutron spin asymmetry data are from the recent SLAC measurement [63].

In the SU(6)-symmetric quark model, the ratio R^{np} and asymmetries A_1^n would be independent of x, taking the values 2/3 and 0, respectively, aside from a mild x dependence of A_1^p resulting from the Melosh transformation. As a result of the symmetry breaking introduced in the present model by OGEP, all the ratios acquire significant x dependence, in reasonable agreement with the trends of the experimental data.

The limiting values at $x \to 1$ of A_1^n , A_1^p, and R^{np} are predicted by perturbative QCD [64] to be 1, 1, 3/7. The present calculation of A_1^p does approach 1 as $x \to 1$. In the neutron case, the spin asymmetry appears to approach 1 for the **56** + **70** wave function but not when the **56′** is included. Away from $x = 1$, the **56′** component fitted to spectroscopy has little effect. Qualitatively this can be understood by noting that the **56′** is a symmetric

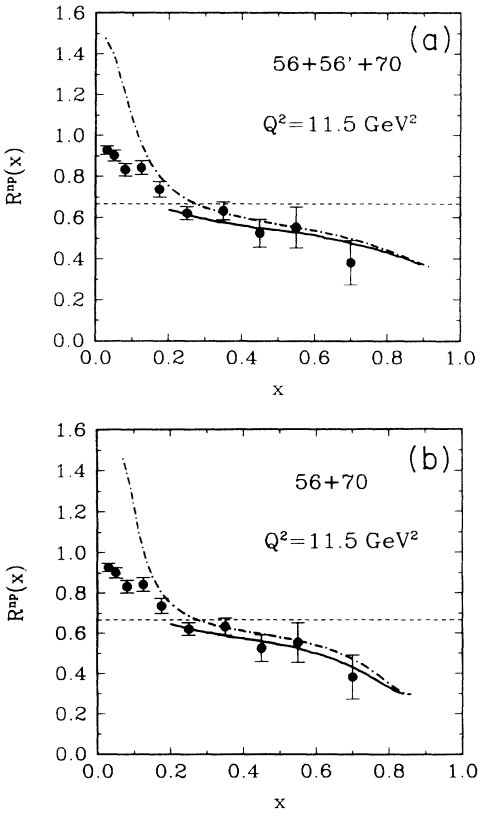

FIG. 5. The ratio of the neutron to proton structure functions compared with the data of Ref. [60]. (a) **56** + **56′** + **70** and (b) **56** + **70**.

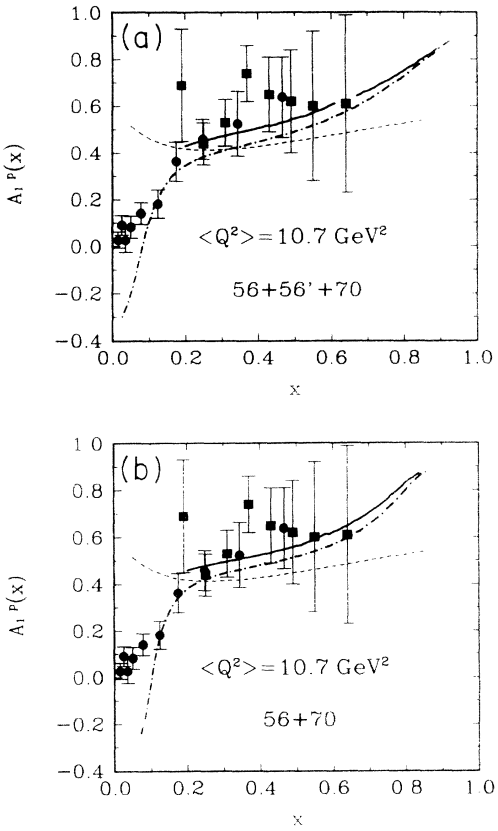

FIG. 6. The proton spin asymmetry compared with the data of Refs. [61, 62]. (a) **56** + **56′** + **70** and (b) **56** + **70**.

but radially excited component, having enhanced high-momentum content compared to the ground state **56**. Thus the **56′** dilutes the symmetry breaking effect of the **70** admixture at the high momentum limit. For R^{np}, the present calculations approach 0.25 at $x \to 1$, rather than $3/7 \sim 0.43$. It is interesting to note that the perturbative QCD estimates of Ref. [64] include SU(6) violation in the photon-quark dynamics, but assume an SU(6)-symmetric structure for the nucleon wave function (**56** configuration only) as $x \to 1$.

The QCD evolution changes the normalization of the valence quark momentum distributions and shifts them toward the small-x values. However, the effect of QCD evolution on the structure function *ratios* in the valence region is rather slight, and the evolved and unevolved ratios are seen to approach each other as $x \to 1$. All of this suggest that the x dependence of neutron to proton structure function ratio and the nucleon asymmetries in the valence region are essentially low Q^2 effects. As Close has observed, "the memory of the constituent quark spins (and flavors) is not lost as one proceeds to the deep inelastic" [65].

We believe that this success of the QCD-inspired quark model indicates that the same spatially dependent color hyperfine interaction which breaks the mass degeneracy of the nucleon and delta is also responsible for inhomogeneity of the quark charge, flavor, and spin distribution within the nucleon.

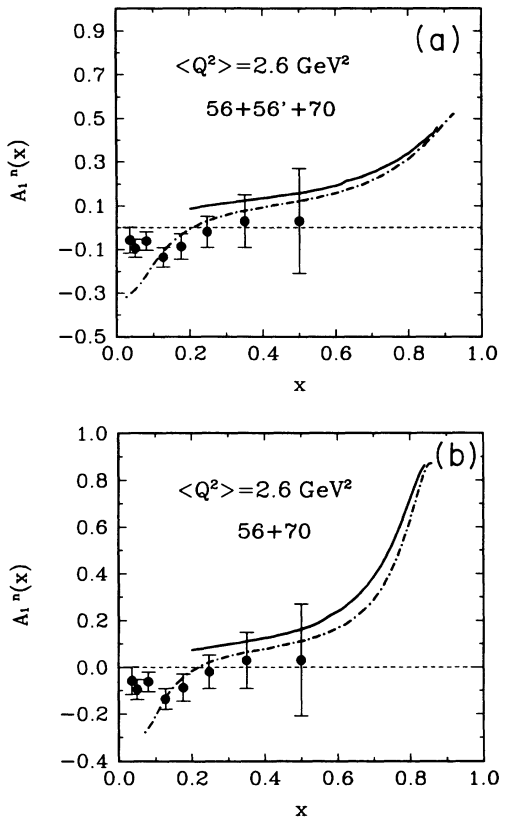

FIG. 7. The neutron spin asymmetry compared with the data of Ref. [63]. (a) **56** + **56'** + **70** and (b) **56** + **70**.

V. DISCUSSION AND SUMMARY

The nonrelativistic quark model was originally formulated to account for the symmetries observed in static properties of baryons. Natural extensions of the model were also able to give a reasonable account of the pattern of symmetry breaking in static properties such as masses and magnetic moments. In the present work, this program has been extended to explain symmetry breaking patterns in deep-inelastic electron- (or muon-)nucleon scattering observables. The principal SU(6) violating effects in deep-inelastic scattering are the x-dependent ratio of proton to neutron F_2 structure functions, and the proton and neutron spin asymmetries. These are shown to be consistent with the same NRQM of the nucleon which fits the static SU(6) breaking.

The success of the present treatment is obtained through use of a transformation from nucleon rest frame momenta to light cone and/or IMF momenta which avoids strong approximations made in previous work. QCD evolution is found to have a non-negligible effect on the quark distributions themselves, but these effects for the most part cancel out in the distribution function ratios which correspond to the observables selected for study.

The present model is deficient in several ways. First, the underlying quark model does not give correct absolute values for the neutron and proton charge radii, although it does give the ratio of these quantities correctly. This problem is likely connected to the model's use of structureless (pointlike) particles as valence quarks and (inaccurate) truncated harmonic oscillator basis. Intimately related to this problem is the fact that the QCD evolution in the present work must be extended to a very low (nonperturbative) momentum scale in order to match the experimental value of F_p^2 at $x = 1/3$. The valence quarks of the NRQM are giving only the "core" of the physical nucleon wave function; the overall size and the normalization can only be accounted for if the pion cloud or sea quark and gluon content are somehow included. The literature contains several reasonably successful approaches to including these effects. However, the approximate spin and flavor symmetry of the sea suggests that its inclusion would not change the results obtained here too much.

The present work identifies, at a low momentum scale, a three-particle Schrödinger wave function in Eq. (14) with the lowest particle-number component of the relativistic Fock space wave function in Eq. (12). The dependent variables of these two functions are then connected using the Lorentz boost of Eqs. (20) and (28). The truncation of basis is still in the nature of a "prescription." This is also the case for all other such transformations in use, because there is an inherent mismatch between the fixed particle number, instant picture of nonrelativistic quantum mechanics, and the indefinite particle number, equal $\xi^+ = t + z$ picture of light-cone dynamics. The advantage of the method developed in the present work is that the kinematical transformations used are obtained from the basic kinematical definitions of the two pictures without introduction of a drastic nonrelativistic approximation as has been done in the past. The present prescription has been shown to reduce in the nonrelativistic and static ($x \to 1/3$) limits, to the prescriptions used in previous works. Only a complete relativistic solution of QCD on the light cone would completely eliminate this deficiency.

Note added in proof. After the submission of this work we received a paper on related work by Weber [66] which shows agreement with our results for the phase of the **56** + **70** wave function admixture and for certain experimental predictions.

ACKNOWLEDGMENTS

We wish to thank Z. E. Meziani for providing experimental data on the neutron spin asymmetry, M. Pindor for the very efficient integration routine FDAI, and J.T. Londergan for the code used to solve the Altarelli-Parisi equations for QCD evolution. One of us (Z.D.) would also like to thank the Institute of Nuclear Theory at the University of Washington for kind hospitality and financial support during the completion of part of this work.

APPENDIX A: FLAVOR AND SPIN WAVE FUNCTIONS IN POSITION AND MOMENTUM SPACE

Explicit formulas for the nucleon spin and flavor wave functions used in the present work are given here.

The proton and neutron flavor wave functions each contain a mixed-symmetry, antisymmetric (ρ) and a mixed- symmetry, symmetric (λ) component. These are given by

$$\varphi_p^\rho = \frac{1}{\sqrt{2}}(udu-duu),\quad \varphi_p^\lambda = \frac{1}{\sqrt{6}}(2uud-duu-udu), \tag{A1}$$

$$\varphi_n^\rho = \frac{1}{\sqrt{2}}(udd-dud),\quad \varphi_n^\lambda = \frac{1}{\sqrt{6}}(udd+dud-2ddu). \tag{A2}$$

The spin wave functions with the corresponding symmetries are given by

$$\chi_\uparrow^\rho = \frac{1}{\sqrt{2}}(\uparrow\downarrow\uparrow - \downarrow\uparrow\uparrow),\quad \chi_\uparrow^\lambda = \frac{1}{\sqrt{6}}(2\uparrow\uparrow\downarrow - \downarrow\uparrow\uparrow - \uparrow\downarrow\uparrow), \tag{A3}$$

$$\chi_\downarrow^\rho = \frac{1}{\sqrt{2}}(\uparrow\downarrow\downarrow - \downarrow\uparrow\downarrow),\quad \chi_\downarrow^\lambda = \frac{1}{\sqrt{6}}(\uparrow\downarrow\downarrow + \downarrow\uparrow\downarrow - 2\downarrow\downarrow\uparrow). \tag{A4}$$

The Jacobi coordinates needed for the radial wave functions are

$$\boldsymbol{\rho} = \frac{1}{\sqrt{2}}(\mathbf{r}_1 - \mathbf{r}_2),\qquad \boldsymbol{\lambda} = \frac{1}{\sqrt{6}}(\mathbf{r}_1 + \mathbf{r}_2 - 2\mathbf{r}_3), \tag{A5}$$

$$\mathbf{p}_\rho = \frac{1}{\sqrt{2}}(\mathbf{p}_1 - \mathbf{p}_2),\qquad \mathbf{p}_\lambda = \frac{1}{\sqrt{6}}(\mathbf{p}_1 + \mathbf{p}_2 - 2\mathbf{p}_3). \tag{A6}$$

We define the function

$$\Phi^S \equiv \Phi_0(\boldsymbol{\rho},\boldsymbol{\lambda}) = \frac{\alpha^3}{\pi^{3/2}}\exp\left(-\frac{\alpha^2}{2}\{\rho^2+\lambda^2\}\right). \tag{A7}$$

Internal wave functions are normalized with respect to the measure $\int d^3\boldsymbol{\rho} d^3\boldsymbol{\lambda}$.

Then the spatial wave functions relevant for the present work are

$$\Phi^{S'} = \frac{\alpha^2}{\sqrt{3}}(\rho^2+\lambda^2-3\alpha^{-2})\,\Phi_0, \tag{A8}$$

$$\Phi^\rho = \frac{2\alpha^2}{\sqrt{3}}\,\boldsymbol{\rho}\cdot\boldsymbol{\lambda}\,\Phi_0, \tag{A9}$$

$$\Phi^\lambda = \frac{\alpha^2}{\sqrt{3}}(\rho^2-\lambda^2)\,\Phi_0. \tag{A10}$$

In the momentum representation, wave functions are normalized with respect to the measure $\int d^3\mathbf{p}_\rho d^3\mathbf{p}_\lambda$. With the definition

$$\Phi^S \equiv \Phi_0(\mathbf{p}_\rho,\mathbf{p}_\lambda) = \frac{\alpha^{-3}}{\pi^{3/2}}\exp\left(-\frac{1}{2\alpha^2}\{p_\rho^2+p_\lambda^2\}\right), \tag{A11}$$

the momentum wave functions used in the present work are

$$\Phi^{S'} = \frac{\alpha^{-2}}{\sqrt{3}}(3\alpha^2 - p_\rho^2 - p_\lambda^2)\,\Phi_0, \tag{A12}$$

$$\Phi^\rho = \frac{2\alpha^{-2}}{\sqrt{3}}(-\mathbf{p}_\rho\cdot\mathbf{p}_\lambda)\,\Phi_0, \tag{A13}$$

$$\Phi^\lambda = \frac{\alpha^{-2}}{\sqrt{3}}(-p_\rho^2 + p_\lambda^2)\,\Phi_0. \tag{A14}$$

To transform wave functions to the light cone, the above relative momentum wave functions must be re-expressed in terms of the individual momenta as

$$\Phi^S(\mathbf{p}_1,\mathbf{p}_2,\mathbf{p}_3) \equiv \Phi_0 = \frac{\alpha^{-3}}{\pi^{3/2}}\exp\left(-\frac{1}{2\alpha^2}\sum\mathbf{p}_i^2\right), \tag{A15}$$

$$\Phi^{S'}(\mathbf{p}_1,\mathbf{p}_2,\mathbf{p}_3) = \frac{\alpha^{-2}}{\sqrt{3}}\left(3\alpha^2 - \sum\mathbf{p}_i^2\right)\,\Phi_0, \tag{A16}$$

$$\Phi^\rho(\mathbf{p}_1,\mathbf{p}_2,\mathbf{p}_3) = \frac{2\alpha^{-2}}{\sqrt{3}}(\mathbf{p}_2^2 - \mathbf{p}_1^2)\,\Phi_0, \tag{A17}$$

$$\Phi^\lambda(\mathbf{p}_1,\mathbf{p}_2,\mathbf{p}_3) = \frac{\alpha^{-2}}{\sqrt{3}}(2\mathbf{p}_3^2 - \mathbf{p}_1^2 - \mathbf{p}_2^2)\,\Phi_0. \tag{A18}$$

APPENDIX B: SPATIAL OVERLAP INTEGRALS

The integrals occurring in the evaluation of quark spatial distributions within the present model are defined here.

With the definitions

$$x = \alpha\, r,\quad f(r) = (3\alpha^2/2\pi)^{3/2}\exp(-1.5x^2), \tag{B1}$$

the overlap integrals needed to evaluate Eqs. (9) in the text are given by

$$\begin{aligned} I_{SS}(r) &= \int d^3\boldsymbol{\rho}\, d^3\boldsymbol{\lambda}\,[\cos\theta\,\Phi^S + \sin\theta\,\Phi^{S'})^2\,\delta^3(\mathbf{r}-\mathbf{r}_3) \\ &= f(r)\,[\cos^2\theta + \sqrt{3}\sin\theta\cos\theta\,(x^2-1) \\ &\quad +\sin^2\theta\,(\tfrac{5}{4} - \tfrac{3}{2}\,x^2 + \tfrac{3}{4}\,x^4)], \end{aligned} \tag{B2}$$

$$\begin{aligned} I_{S\lambda}(r) &= \int d^3\boldsymbol{\lambda}\,(\cos\theta\,\Phi^S + \sin\theta\,\Phi^{S'})\,\Phi^\lambda\,\delta^3(\mathbf{r}-\mathbf{r}_3) \\ &= f(r)\,\left(\cos\theta\,\frac{\sqrt{3}}{2}\,(1-x^2)\right. \\ &\quad \left. +\sin\theta\,(-\tfrac{1}{4} + \tfrac{3}{2}\,x^2 - \tfrac{3}{4}\,x^4)\right), \end{aligned} \tag{B3}$$

$$\begin{aligned} I_{\lambda\lambda}(r) &= \int d^3\boldsymbol{\rho}\, d^3\boldsymbol{\lambda}\,(\Phi^\lambda)^2\,\delta^3(\mathbf{r}-\mathbf{r}_3) \\ &= f(r)\,(\tfrac{5}{4} - \tfrac{3}{2}\,x^2 + \tfrac{3}{4}\,x^4), \end{aligned} \tag{B4}$$

$$I_{\rho\rho}(r) = \int d^3\boldsymbol{\rho}\, d^3\boldsymbol{\lambda}\,(\Phi^\rho)^2\,\delta^3(\mathbf{r}-\mathbf{r}_3) = f(r)\,x^2. \tag{B5}$$

APPENDIX C: FLAVOR AND SPIN ASYMMETRIES

The spin average and spin weighted nucleon structure functions are given in terms of quark charges and distribution functions by the standard definitions

$$F_1(x,Q^2) = \frac{1}{2}\sum_i e_i^2\, q_i(x,Q^2), \tag{C1}$$

$$g_1(x,Q^2) = \frac{1}{2}\sum_i e_i^2\, \Delta q_i(x,Q^2), \tag{C2}$$

$$q = q_\uparrow + \bar{q}_\uparrow + q_\downarrow + \bar{q}_\downarrow, \tag{C3}$$

$$\Delta q = q_\uparrow + \bar{q}_\uparrow - q_\downarrow - \bar{q}_\downarrow, \tag{C4}$$

$$A_1(x,Q^2) = \frac{g_1(x,Q^2)}{F_1(x,Q^2)}, \tag{C5}$$

$$R^{np}(x,Q^2) = \frac{F_1^n(x,Q^2)}{F_1^p(x,Q^2)}. \tag{C6}$$

Here the index i refers to quark flavor, and the bar over a distribution refers to the corresponding antiquark distribution, generated by the QCD evolution procedure. Note that the anomaly contribution to g_1 is neglected, although the present model does in principle permit calculation of the gluon polarization.

[1] For a recent review of the light-cone quantization technique of QCD, see S. J. Brodsky and H-Ch. Pauli, in *Recent Aspects of Quantum Fields*, edited by H. Mittev and H. Gausterer, Lecture Notes in Physics **396** (Springer-Verlag, 1992).

[2] A report of this work has been given by Z. Dziembowski, C. J. Martoff, and P. Żyła, in *International Symposium on Spin-Isospin Response in Hadrons and Nuclei*, Osaka, Japan, edited by H. Ejiri, Y. Mizuno, and T. Suzuki [Nucl. Phys. A (in press)].

[3] A. De Rújula, H. Georgi, and S. L. Glashow, Phys. Rev. D **12**, 147 (1975).

[4] N. Isgur and G. Karl, Phys. Lett. **72B**, 109 (1977); **74B**, 353 (1978); Phys. Rev. D **18**, 4187 (1978); **19**, 2653 (1979); **20**, 1119 (1979).

[5] F. E. Close, Phys. Lett. **43B**, 422 (1973).

[6] R. Carlitz, Phys. Lett. **58B**, 345 (1975).

[7] A. Le Yaouanc, L. Oliver, O. Pène, and J. C. Raynal, Phys. Rev. D **11**, 680 (1975); **12**, 2137 (1975); **13** 1519(E) (1976).

[8] F. E. Close and A. W. Thomas, Phys. Lett. B **212**, 227 (1988).

[9] Z. Dziembowski, L. Mankiewicz, A. Szczepaniak, and H. J. Weber, Phys. Rev. D **39**, 3257 (1989).

[10] L. Susskind, Phys. Rev. **165**, 1535 (1968); in *Lectures in Theoretical Physics*, Vol. 11d, edited by K. Mahanthappa and W. Brittin (Gordon and Breach, New York, 1969).

[11] J. B. Kogut and D. E. Soper, Phys. Rev. D **1**, 2901 (1970); D. E. Soper, SLAC Report No. 137, 1971 (unpublished).

[12] A. Le Yaouanc, L. Oliver, O. Pène, and J. C. Raynal, Phys. Rev. D **15**, 844 (1976); see Eq. (2.12) and the discussion below Eq. (2.16) in this reference.

[13] A. Le Yaouanc, L. Oliver, O. Pène, and J. C. Raynal, Phys. Rev. D **18**, 1733 (1978).

[14] F. E. Close, *Introduction to Quarks and Partons* (Academic, New York, 1978).

[15] A. Le Yaouanc, L. Oliver, O. Pène, and J. C. Raynal, *Hadron Transitions in the Quark Model* (Gordon and Breach, New York, 1988).

[16] A. Manohar and H. Georgi, Nucl. Phys. **B234**, 189 (1984).

[17] T. DeGrand, R. L. Jaffe, K. Johnson, and J. Kiskis, Phys. Rev. D **12**, 2060 (1975).

[18] A. Le Yaouanc, L. Oliver, O. Pène, and J. C. Raynal, Phys. Rev. D **18**, 1591 (1978).

[19] N. Isgur, G. Karl, and R. Koniuk, Phys. Rev. Lett. **41**, 1269 (1978); *ibid.* **45**, 1738(E) (1980).

[20] S. Capstick and N. Isgur, Phys. Rev. D **34**, 2809 (1986); S. Capstick, *ibid.* **46**, 1965 (1992).

[21] R. D. Carlitz, S. D. Ellis, and R. Savit, Phys. Lett. **68B**, 443 (1977).

[22] N. Isgur, Acta Phys. Polon. **B8**, 1081 (1977).

[23] J. F. Donoghue and G. Karl, Phys. Rev. D **24**, 230 (1981).

[24] S. J. Brodsky and J. R. Primack, Ann. Phys. (N.Y.) **52**, 315 (1969); S. J. Brodsky and S. D. Drell, Phys. Rev. D **22**, 2236 (1980).

[25] R. Nag, S. Sanyal, and S. N. Mukherjee, Prog. Theor. Phys. **83**, 51 (1990); B. N. Mukherjee *et al.*, Phys. Rep. **231**, 201 (1993).

[26] A. W. Thomas, S. Théberge, and G. A. Miller, Phys. Rev. D **24**, 216 (1981).

[27] Z. Dziembowski and L. Mankiewicz, Phys. Rev. D **36**, 1556 (1987).

[28] Z. Dziembowski, in *Quark Cluster Dynamics*, Lecture Notes in Physics, Vol. 417, edited by K. Goeke, P. Kroll, and H.-R. Petry (Springer-Verlag, Berlin, Heidelberg, 1992).

[29] R. Brandt, Phys. Rev. Lett. **23**, 1260 (1969); B. L. Ioffe, Phys. Lett. **30B**, 123 (1969).

[30] P. A. M. Dirac, Rev. Mod. Phys. **21**, 392 (1949).

[31] H. Leutwyler and J. Stern, Ann. Phys. (N.Y.) **112**, 94 (1978).

[32] S. D. Drell and T. M. Yan, Phys. Rev. Lett. **24**, 181 (1970).

[33] Cl. Bouchiat, P. Fayet, and P. Meyer, Nucl. Phys. **B34**, 157 (1971).

[34] S. Weinberg, Phys. Rev. **150**, 1313 (1966).

[35] L. A. Kondratyuk and M. V. Terentev, Yad. Fiz. **31**, 1087 (1980) [Sov. J. Nucl. Phys. **31**, 561 (1980)].

[36] H. J. Melosh, Phys. Rev. D **9**, 1095 (1974).

[37] J. D. Bjorken and S. D. Drell, *Relativistic Quantum Mechanics* (McGraw-Hill, New York, 1964).

[38] Note that the infinite momentum spinors introduced in Eq. (4.51) of Ref. [11] are given in the Weyl or chiral realization of the γ matrices rather than in the Dirac represention used in the present work.

[39] S. Glazek, Acta Phys. Polon. **B15**, 889 (1984).

[40] V. B. Berestetskiĭ and M. V. Terentev, Yad. Fiz. **24**, 1044 (1976) [Sov. J. Nucl. Phys. **24**, 547 (1976)].
[41] C. J. Brodsky, T. Huang, and G. P. Lepage, in *Quarks and Nuclear Forces*, Springer Tracts in Modern Physics, Vol. 100, edited by D. Fries and B. Zeitnitz (Springer-Verlag, New York, 1982).
[42] Z. Dziembowski, Phys. Rev. D **37**, 768 (1988); **37**, 778 (1988).
[43] See Eq. (3.12) in Ref. [41].
[44] See Refs. [9, 28, 42] and also Z. Dziembowski and L. Mankiewicz, Phys. Rev. Lett. **58**, 2175 (1987); J. Bienkowska, Z. Dziembowski, and H. Weber, *ibid.* **59**, 624 (1987); **59**, 1790(E) (1987); Z. Dziembowski, Phys. Rev. D **37**, 2030 (1988); Z. Dziembowski and J. Franklin, *ibid.* **42**, 905 (1990).
[45] W. Konen and H. J. Weber, Phys. Rev. D **41**, 2201 (1990); H. J. Weber, Phys. Rev. C **41**, 2783 (1990); Ann. Phys. (N.Y.) **207**, 417 (1991); Phys. Lett. B **287**, 14 (1992).
[46] C. R. Ji and S. R. Cotanch, Phys. Rev. D **41**, 2319 (1990); C. R. Ji and F. Amiri, *ibid.* **42**, 3764 (1990); C. R. Ji, P. L. Chung, and S. R. Cotanch, *ibid.* **45**, 4214 (1992).
[47] Restoring the nonstatic value of $\mu_q = 1/(p_0 + m)$ in Eqs. (3.3) and (3.4) of the first and second papers of Ref. [7], respectively, one gets a result that disagrees with the IMF spinors of Refs. [11, 38].
[48] V. B. Berestetski and M. V. Terentev, Yad. Fiz. **25**, 653 (1977) [Sov. J. Nucl. Phys. **25**, 347 (1977)]; I. G. Aznauryan, A. B. Bagdasaryan, and N. L. Ter-Isaakyan, *ibid.* **36**, 1278 (1982) [**36**, 743 (1982)]; F. Coester, Prog. Part. Nucl. Phys. **29**, 1 (1992).
[49] G. P. Lepage, J. Comput. Phys. **27**, 192 (1978); see also W. H Press, B. P. Flannary, S. A. Teukolsky, and W. T. Vetterling, *Numerical Recipes*, 2nd ed. (Cambridge University Press, Cambridge, England, 1992).
[50] A. Dydek and M. Pindor, Warsaw University Report No. IFT/11/78 (unpublished).
[51] S. Wolfram, *Mathematica, a System for Doing Mathematics by Computer* (Addison-Wesley, New York, 1991).
[52] J. D. Jackson, G. G. Ross, and R. G. Roberts, Phys. Lett. B **226**, 159 (1989).
[53] R. L. Jaffe and G. G. Ross, Phys. Lett. **93B**, 313 (1980).
[54] C. J. Benesh and G. A. Miller, Phys. Rev. D **36**, 1344 (1987); **38**, 48 (1988), Phys. Lett. B **215**, 381 (1988); F. W. Schreiber, A. W. Thomas, and J. T. Londergan, Phys. Rev. D **42**, 2226 (1990); A. W. Schreiber, A. I. Signal, and A. W. Thomas, *ibid.* **44**, 2653 (1991); H. Meyer and P. J. Mulders, Nucl. Phys. **A528**, 589 (1991).
[55] V. N. Gribov and L. N. Lipatov, Yad. Fiz. **15** , 781 (1972) [Sov. J. Nucl. Phys. **15**, 438 (1972)]; **15**, 1218 (1972) [**15**, 675 (1972)]; G. Altarelli and G. Parisi, Nucl. Phys. **B126**, 298 (1977).
[56] S. Kumano and J. T. Londergan, Comput. Phys. Commun. **69**, 373 (1992).
[57] D. J. Gross, Phys. Rev. Lett. **32**, 1071 (1974); R. D. Field, *Applications of Perturbative QCD* (Addison-Wesley, New York, 1989).
[58] NMC, P. Amaudruz *et al.,* Phys. Lett. B **295**, 159 (1992).
[59] M. Glück, R. M. Godbole, and E. Reya, Z. Phys. C **41**, 667 (1989); M. Glück, E. Reya, and A. Vogt, *ibid.* **48**, 471 (1990); **53**, 127 (1992).
[60] NMC, P. Amaudruz *et al.*, Nucl. Phys. **B371**, 3 (1992).
[61] G. Baum *et al.*, Phys. Rev. Lett. **51**, 1135 (1981).
[62] EM Collaboration, J. Ashman *et al.*, Nucl. Phys. **B328**, 1 (1989).
[63] E142 Collaboration, P. L. Anthony *et al.*, Phys. Rev. Lett. **71**, 959 (1993); also Z. E. Meziani (private communication).
[64] G. R. Farrar and D. R. Jackson, Phys. Rev. Lett. **35**, 1416 (1975); B. L. Ioffe, V. A. Khoze, and L. N. Lipatov, *Hard Processes* (North-Holland, Amsterdam, 1984), Vol. 1.
[65] F. Close, Nucl. Phys. **A508**, 413c (1990).
[66] H. J. Weber, Phys. Rev. D **49**, 3160 (1994).